arXiv:1403.6586v1 [cond-mat.mes-hall] 26 Mar 2014

# Microwave nanobolometer based on proximity Josephson junctions

J. Govenius,[1,*] R. E. Lake,[1] K. Y. Tan,[1] V. Pietilä,[1] J. K. Julin,[2] I. J. Maasilta,[2] P. Virtanen,[3] and M. Möttönen[1,3]

[1]*QCD Labs, COMP Centre of Excellence, Department of Applied Physics, Aalto University, P.O. Box 13500, FIN-00076 Aalto, Finland*

[2]*Nanoscience Center, Department of Physics, P.O. Box 35, FIN-40014 University of Jyväskylä, Finland*

[3]*O. V. Lounasmaa Laboratory, Aalto University, P.O. Box 15100, FIN-00076 Aalto, Finland*

(Dated: March 27, 2014)

We introduce a microwave bolometer aimed at high-quantum-efficiency detection of wave packet energy within the framework of circuit quantum electrodynamics, the ultimate goal being single microwave photon detection. We measure the differential thermal conductance between the detector and its heat bath, obtaining values as low as 5 fW/K at 50 mK. This is one tenth of the thermal conductance quantum and corresponds to a theoretical lower bound on noise-equivalent-power of order $10^{-20}$ W/$\sqrt{\text{Hz}}$ at 50 mK. By measuring the differential thermal conductance of the same bolometer design in qualitatively different environments and materials, we determine that electron–photon coupling dominates the thermalization of our nanobolometer.

Reaching noise-equivalent-power (NEP) of $10^{-20}$ W/$\sqrt{\text{Hz}}$ in radiation sensors is an important goal for space-based telescopy because it allows cosmic background radiation limited spectroscopy in the THz regime [1, 2]. What intrigues us however, is that such low noise levels would also enable direct measurement of wave packet energy in circuit quantum electrodynamics (cQED) [3, 4]. For example, NEP of $10^{-21}$ W/$\sqrt{\text{Hz}}$ allows resolving an individual 10 GHz microwave photon emitted from a qubit or resonator with energy relaxation time of 10 $\mu$s. Even a more modest NEP of $10^{-18}$ W/$\sqrt{\text{Hz}}$ enables on-chip phase-insensitive energy measurements of multi-photon wave packets, such as dispersive qubit measurement pulses [3, 5]. Since the energy of a wave packet and the voltage produced by it correspond to non-commuting quantum-mechanical observables, such single-shot energy measurements are fundamentally impossible with traditional microwave amplifiers which amplify voltage [6]. In addition to low NEP, these measurements require high bandwidth and absorption of nearly all of the incident microwave radiation, i.e., high quantum efficiency. To the best of our knowledge, no detector simultaneously satisfying all of these criteria has been reported.

Transition edge sensors (TES) [1, 7–11] and kinetic inductance detectors [12, 13] are the most mature bolometer technologies. Use of other superconductor weak links [14–17], semiconductor nanostructures [18–20], graphene [21–24], carbon nanotubes [25], and quantum capacitance [26–28] has also been experimentally explored. State-of-the-art TESs [8] and semiconducting detectors [20] have reached phenomenal NEP at THz frequencies but at radio frequencies (rf) these detectors are reactive rather than resistive [29], which makes absorbing microwave photons from transmission lines used in cQED inefficient. Furthermore, they are typically read out using low-bandwidth amplifiers [7, 8, 20]. Our hot-electron [30] nanobolometer addresses these issues by electrically isolating the absorber and thermometer components and by providing an rf coupled readout. The former enables efficient matching to an input microwave transmission line, while the latter allows frequency multiplexing and use of low-noise rf amplifiers at the output [6].

We report on heat conductance measurements between our nanobolometer and its heat bath. By measuring the same bolometer design in different electromagnetic environments and by using different materials, we find that the dominant heat link between our sensor and the environment is the electron–photon thermal conductance. Like other single mode conduction channels, the electron–photon conductance is bound from above by the universal heat conductance quantum $G_Q = \pi^2 k_b^2 T/3h$ [31–35], which is reached when the detector and environment impedances are matched at thermal excitation frequencies [36]. By engineering the electromagnetic environment in the vicinity of the sensor, we reduce the total differential thermal conductance to $0.1 \times G_Q = 5$ fW/K at 50 mK. This is an important result since it implies that the theoretical lower bound on NEP set by thermal energy fluctuations [7, 37–39] is of order $10^{-20}$ W/$\sqrt{\text{Hz}}$ for our sensor. We note that similar heat conductivities have been previously achieved in suspended TESs [9] and even lower values in a hot-electron TES [7], but without impedance matching at microwave input frequencies and with substantially lower readout bandwidth. Furthermore, our detector demonstrates experimentally the temperature to inductance transduction mechanism proposed in the so called Josephson proximity sensor [40, 41].

The central component of our nanobolometer is a diffusive normal-metal nanowire contacted by three superconductor leads, which together form two diffusive superconductor–normal-metal–superconductor (SNS) junctions with a total normal-metal volume of order $(100\,\text{nm})^3$ [see Fig. 1(b) and Table I]. We fabricated all nanowires with electron beam lithography using shadow angle evaporation of $\text{Au}_x\text{Pd}_{1-x}$ as normal metal and Al or Nb as superconductor on oxidized silicon substrates. We estimate $x \approx 0.75$ based on evaporation parameters and known alloy stabilities [42]. Electrical measurements were performed in a cryostat with base temperature of 10 mK. At a bath temperature of 100 mK, the long junction is an ohmic resistor $R_{N,\text{long}}$ in all samples, while the short junction supports a non-dissipative supercurrent with clear switching and retrapping at currents of order 100 nA. Even at 10 mK, the long junction shows a mere reduced re-

sistance at the smallest currents ($< 10$ nA) but no switching. This allows us to neglect the reactive component of the long junction admittance.

Samples A, B, C, and N were dc coupled and measured using sub-kHz frequencies [dc mode, Fig. 1(c)], while Samples R and F were capacitively coupled and measured at microwave frequencies [rf mode, Fig. 1(d)]. Shunting lead G [Fig. 1(b)] to ground through a small resistance in dc mode and by a large capacitor ($C_1$) in rf mode provides electrical isolation between the long and short junctions, but does not prevent thermalization between the junctions on relevant timescales [43, 44]. Therefore, a single temperature $T_e$ accurately describes the electronic system of the entire normal-metal nanowire. In all samples, the long junction heats the electron gas ($P_{\text{local}}$) while the short junction transduces $T_e$ into an electrical signal. In dc mode, a fixed current bias heats the electrons with $P_{\text{local}} = I_{\text{long}}^2 R_{N,\text{long}}$, while the current at which the short junction switches from the superconducting state to the normal state indicates electron temperature. In rf mode, a transmission line delivers $P_{\text{local}}$ at several GHz, while a small amplitude excitation at hundreds of MHz probes the $T_e$ dependent inductance of the short junction.

More specifically, in dc mode we ramp the current bias through the short junction $I_{\text{short}}(t)$ linearly over several milliseconds while measuring voltage $V$ over it in a four-wire configuration. As the short SNS junction switches from the superconducting state to the normal state, $V$ jumps from zero to $I_{\text{short}} R_{\text{N,short}}$ at a stochastic time $t_{\text{switch}}$. Since the ramp is much slower than the inverse bandwidth of our electrical lines, we can convert $t_{\text{switch}}$ directly to a current $I_{\text{short}}(t_{\text{switch}})$. We repeat this $I_{\text{short}}$ bias cycle approximately $10^3$ times and record a histogram of switching currents [Fig. 2(a)] as well as the voltage trace averaged over all repetitions. We then define either the median of the switching current distribution or the current at which $V$ on average crosses $0.5 \times I_{\text{short}} R_{\text{N,short}}$ as a typical switching current $I_s^\star$. This $I_s^\star$ defines an uncalibrated electron temperature probe $A(T_e)$ [Fig. 1(a)] in dc mode. It is challenging to accurately infer the theoretical critical current $I_c$ or the absolute temperature $T_e$ based on $I_s^\star$ without drastically simplified theoretical models [45, 46]. This is not problematic here, however, since $A(T_e)$ does not need to be calibrated (discussed below). Note also that the heating current $I_{\text{long}} \ll I_s^\star$, meaning that heating affects the temperature probe only through $T_e$.

For Sample R (F), the long junction absorbs $P_{\text{local}}$ from a monochromatic 8.8 (6.74) GHz coherent excitation applied between H and G [Fig. 1(d)]. The heating tone is generated by a room-temperature microwave generator and delivered to the sample through fifty-ohm coaxial transmission lines, a number of commercial attenuators and filters inside the cryostat, and finally a symmetrically coupled on-chip coplanar waveguide (CPW) resonator with a fundamental resonance frequency equal to the heater frequency. We calibrated the attenuation of the commercial components, assumed negligible attenuation for resonant transmission through the overcoupled CPW resonator [47], and estimated $R_{\text{N,long}}$ based on

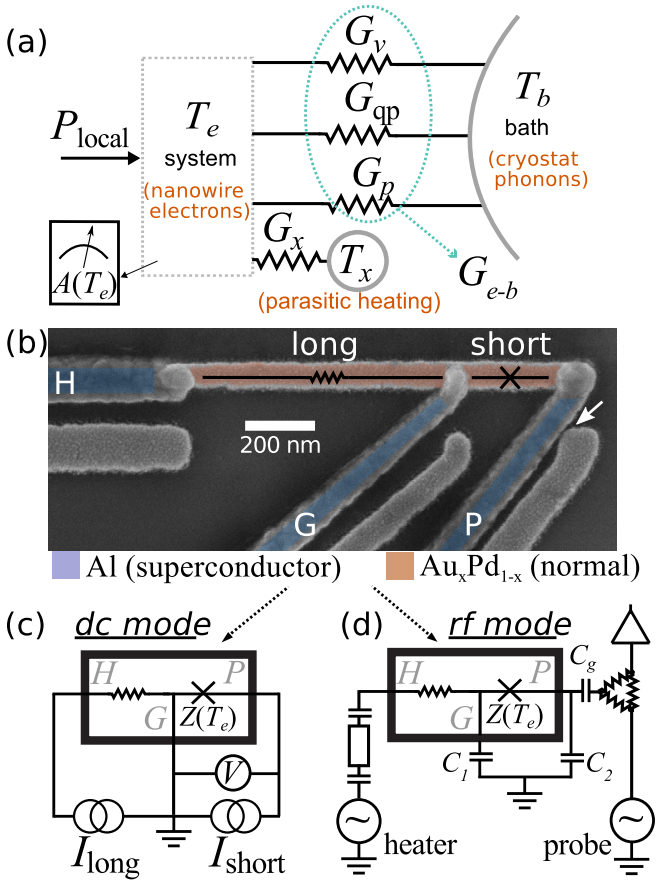


FIG. 1. (Color online) (a) Thermal model of the electron system at temperature $T_e$ coupled to a bath at $T_b$ through photonic ($G_\nu$), quasiparticle ($G_{\text{qp}}$), and phononic ($G_p$) thermal conductances that comprise the total conductance ($G_{e-b}$). $G_x$ quantifies coupling to a parasitic bath ($T_x$). $P_{\text{local}}$ is local heating power, and $A(T_e)$ is a temperature-dependent observable. (b) Micrograph of Sample A. The normal-metal nanowire is contacted by three superconductor leads: heater (H), ground (G) and temperature probe (P). The white arrow indicates an unintentional galvanic contact present only in Sample A. (c) Simplified electrical schematic for measurement of the temperature-dependent sensor impedance $Z(T_e)$ in Samples A, B, C, and N (dc mode). (d) Same for Samples R and F (rf mode).

resistivities of the dc coupled samples in order to take into account the small ($\sim$15%) amount of power reflected due to $R_{\text{N,long}} > 50\,\Omega$.

In rf mode, we probe the electron temperature through the reflection coefficient of a tank circuit that consists of on-chip parallel plate capacitors $C_1 \sim 100$ pF, $C_2$, and $C_g$ together with the mostly reactive admittance $Z(T_e)^{-1}$ of the short SNS junction [Fig. 1(d)]. For Sample R (F), $C_1 = 25C_2 = 75C_g$ ($C_1 = C_2 = 10C_g$). In the rf mode samples the short junction in fact consists of six SNS junctions made of alternating $150-200$ nm pieces of superconductor and normal-metal, but they are treated as one effective admittance in this Letter. In linear response, the tank circuit in Sample R (F) is a harmonic oscillator with a resonance frequency $f_0 \approx 1/\left(2\pi\sqrt{LC}\right)$ of 1.3 GHz (430 MHz) and quality factor of ten (hundred). Here

$C^{-1} = C_1^{-1} + C_2^{-1}$ and $L = -1/(\omega\,\mathrm{Im}\{Z(T_e)^{-1}\}) \sim 1$ nH is the effective junction inductance at angular frequency $\omega$. The quality factor is governed by the external coupling capacitor $C_g$ and internal losses within the resonator [48, 49]. As the junction heats up, $L \propto 1/I_c$ increases and hence $f_0$ decreases. We define $f_0$ as $A(T_e)$ in rf mode and extract it by measuring the reflection over a range of frequencies near $f_0$. The measurement signal is generated and digitized at room temperature, but high-temperature noise reaching the sample is heavily attenuated by a number of attenuators and amplifiers inside the cryostat. We separate the input and output of the reflection measurement with a resistive splitter and isolate the sample from amplifier noise with attenuators. These should be replaced by circulators in future bolometric applications requiring high signal-to-noise ratio.

We define the differential thermal conductance between the nanowire electrons ($e$) and cryostat phonons ($b$) as:

$$\tilde{G}_{e-b} = -\frac{\partial P_{e-b}(T_e, T_b)}{\partial T_b}, \tag{1}$$

where $P_{e-b} = (T_e - T_b)G_{e-b}$ is the net power flow from $e$ to $b$ and $G_{e-b}(T_e, T_b)$ is the non-differential thermal conductance [Fig. 1(a)]. Our definition is closely related to previous definitions of differential [37] or dynamic [50] thermal conductance, but with the roles of $T_e$ and $T_b$ exchanged. In steady state, the temperatures satisfy the power balance equation:

$$P_{\mathrm{local}} + P_x(T_e, T_x) = P_{e-b}(T_e, T_b) \tag{2}$$

where $P_x = (T_x - T_e)G_x$ quantifies parasitic heating due to an unintentional weak coupling $G_x$ to an independent temperature bath ($T_x$). Because $\tilde{G}_{e-b}$ is independent of this parasitic heating, we can compare it directly to the theoretical predictions for different channels, such as $\tilde{G}_{e-b} = \pi^2 k_b^2 T_b/3h$ for matched single-channel conduction or $\tilde{G}_{e-b} = 5\Sigma V_0 T_b^4$ for electrons thermalized by bulk phonons in a metal of volume $V_0$ and coupling strength $\Sigma$. Note that $T_e$ appears in these predictions only for non-linear channels that include cross terms of $T_b$ and $T_e$ in $P_{e-b}$. By measuring $\tilde{G}_{e-b}$, we can therefore experimentally investigate which thermalization channels dominate, even without a calibrated $T_e$ sensor. Furthermore, $\tilde{G}_{e-b}$ is the correct quantity for estimating the thermal-energy-fluctuation limited NEP due to coupling to $T_b$, which we consider to be of greater interest than fluctuations in the parasitic heating.

Our method of obtaining $\tilde{G}_{e-b}$ is based on mapping contours of constant $A(T_e)$ in the $(T_b, P_{\mathrm{local}})$-plane. Specifically, $-\tilde{G}_{e-b}$ is given by the slope of a contour of $A(T_e)$ in the $(T_b, P_{\mathrm{local}})$-plane, as seen by differentiating Eq. (2) with respect to $T_b$ while holding $T_e$ constant. This is the same principle as in the so called isothermal technique used previously in TES-type samples [51–53], except that we take parasitic heating into account and therefore need to distinguish $\tilde{G}_{e-b}$ from $G_{e-b}$ even in the $P_{\mathrm{local}} \to 0$ limit.

We apply the method described above to the measured typical switching currents shown in Figure 2(b) for Sample A. In order to draw smooth contours of $A(T_e)$, we fit a phenomenologically chosen smooth function $I_s^\star(T_b, P_{\mathrm{local}})$ to the data points; the details of the smoothing function do not affect the extracted $\tilde{G}_{e-b}$ averaged over a $T_b$-scale larger than the data point spacing. We then compute $-\partial P_{\mathrm{local}}/\partial T_b = \tilde{G}_{e-b}$ in the $P_{\mathrm{local}} \to 0$ limit for many such contours and show the resulting curve in Fig. 3, along with the results from all other samples. The results are similar for gradients computed at non-zero $P_{\mathrm{local}}$ (not shown). In the remaining paragraphs, we analyze Fig. 3 in terms of contributions arising from the nanowire electrons being coupled to substrate phonons [30], photons in the electromagnetic environment [34, 36], and quasiparticles in the superconductor leads [54, 55]. We do not expect a measurable contribution from phase slips in the leads [56].

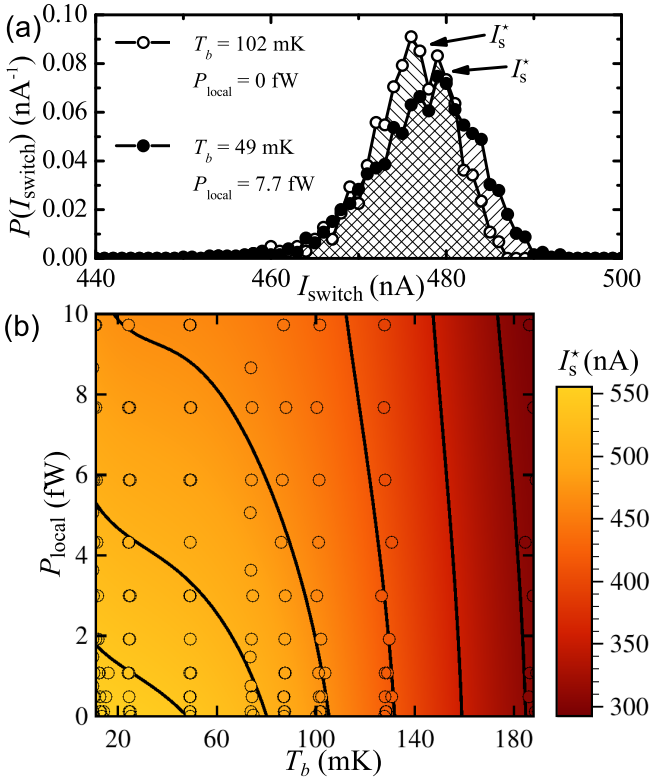


FIG. 2. (Color online) (a) Switching probability density as a function of current through the short SNS junction. The arrows indicate the extracted typical switching currents $I_s^\star$. (b) Measured $I_s^\star$ (color inside circles) at different bath temperatures $T_b$ and heating powers $P_{\mathrm{local}}$. Black curves indicate contours of constant $A(T_e) = I_s^\star$, as determined from a smoothing function (color outside circles). Both panels are for Sample A (Table I).

Coupling of the nanowire electrons to substrate phonons is expected to contribute $5\Sigma V_0 T_b^4 = G_p$ to $\tilde{G}_{e-b}$, where $\Sigma \approx (3 \pm 1) \times 10^9$ W/m$^3$K$^5$ for $Au_{.75}Pd_{.25}$ [57, 58] and $V_0 = (100\,\mathrm{nm})^3$ is a typical volume of our nanowires. This leads to the estimate $\tilde{G}_p = 2$ fW/K at $T_b = 100$ mK, which is one to two orders of magnitude less than the measured values. Furthermore, the observed scaling of $\tilde{G}_{e-b}$ is much weaker than $T_b^4$ at the lowest temperatures (Fig. 3), suggesting that the

TABLE I. Geometric and electric parameters for the long and short sections [Fig. 1(b)] of the nanowire in each sample. $t$ is the nanowire thickness measured by a quartz crystal deposition monitor. We extracted lengths and widths from micrographs and measured the normal-state resistance $R_N$ at $T_b = 10$ mK in dc mode. In rf mode, $R_N$ is an estimate based on size and typical resistivity.

| | | *Long section* | | | *Short section* | | | $T_b = 70$ mK |
|---|---|---|---|---|---|---|---|---|
| sample | t (nm) | length (nm) | width (nm) | $R_N$ ($\Omega$) | length (nm) | width (nm) | $R_N$ ($\Omega$) | $\tilde{G}_{e-b}$ (fW/K) |
| A | 20 | 720 | 80 | 120 | 250 | 100 | 40 | 130 |
| B | 20 | 980 | 150 | 80 | 310 | 140 | 30 | 40 |
| C | 20 | 750 | 50 | 300 | 273 | 60 | 100 | 30 |
| N(Nb) | 60 | 1700 | 440 | 6.8 | 180 | 440 | 4.3 | 80 |
| R | 25 | 1400 | 140 | 100 (est.) | 6 × 180 | 200 | | 10 |
| F | 20 | 1400 | 130 | 130 (est.) | 6 × 180 | 140 | | 10 |

phonon channel is insignificant for Samples B, C, R, and F. Above 80 mK, Samples A and N on the other hand approach the expected dependence for thermalization via phonons in a volume of $130 \times (100\ \text{nm})^3$. Sample N is by design much larger [$70 \times (100\ \text{nm})^3$] than the other nanowires and micrographs of Sample A revealed a galvanic contact between the Al lead for the short junction and the tip of the corresponding normal-metal shadow [Fig. 1(b)]. In that case, thermal resistance over the short superconducting link between the nanowire and the shadow is negligible [43] and thermalization is limited by electron-phonon coupling in the combined nanowire–shadow volume of approximately $130 \times (100\ \text{nm})^3$, leading to results comparable to [59].

In the quasiparticle channel, electrons with energy higher than the superconductor energy gap $\Delta$ diffuse into the three superconductor leads [55]. The thermal conductance for long superconductor leads is suppressed from the normal state value by a factor of $6(y^2 + 2y + 2)e^{-y}/\pi^2$ where $y = \Delta/(k_B T_{\text{qp}})$ [43, 44, 60]. At quasiparticle temperature $T_{\text{qp}} = 100$ mK this corresponds to only a few aW/K even for Al. However, the effective $T_{\text{qp}}$ can be much higher than $T_b$ [54, 61, 62], so we chose to increase $\Delta$ in Sample N by using Nb instead of Al. Since at low temperatures $\tilde{G}_{e-b}$ for Sample N is similar to the other dc mode samples (Fig. 3), we conclude that quasiparticles in the superconductor leads do not significantly add to the total heat conductance. This argument also applies to quasiparticles excited by multiple Andreev reflections [63].

Electron–photon coupling contributes a volume and material independent term to $\tilde{G}_{e-b}$, with a theoretical maximum value of $2G_Q \propto T_b$ in our three-terminal samples. We indeed observe approximately linear $T_b$ scaling in the low-temperature regime in Fig. 3 (except for Sample A), while the prefactors are significantly smaller than two. This is consistent with thermalization through poor but non-vanishing matching of the sample and environment impedances over a broad range of thermally excited frequencies. Furthermore, the prefactor in front of $G_Q$ is notably smaller for rf samples ($\sim$0.1) than dc samples ($\sim$0.5) which differ essentially only in their coupling to the electromagnetic environment. Therefore, we conclude that electron–photon coupling is the dominant thermalization mechanism for our nanobolometer operated in the temperature regime relevant for cQED.

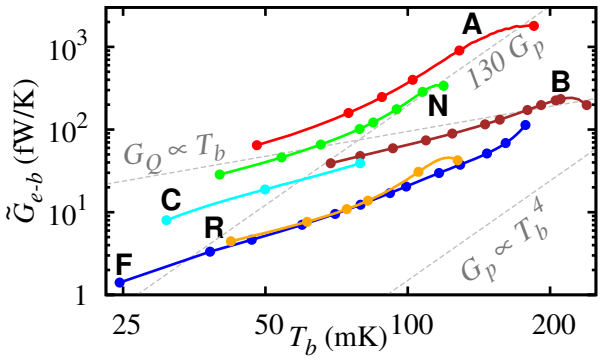


FIG. 3. (Color online) Differential thermal conductance $\tilde{G}_{e-b}(T_b)$ (solid curves) for dc samples (A, B, C, and N) and rf samples (R and F) against bath temperature $T_b$. Each point indicates the $T_b$ value for a set of measured data [see Fig. 2(b)]. The dashed lines show the single-mode quantum of thermal conductance $G_Q$ and the phonon contribution $G_p$ for a typical nanowire volume of $(100\ \text{nm})^3$ and for a large volume of $130 \times (100\ \text{nm})^3$.

In conclusion, we introduced a hot-electron nanobolometer integrated with a microwave transmission line input and a wide-bandwidth rf readout. We measured the differential thermal conductance for multiple samples in qualitatively different materials and electromagnetic environments and found electron–photon coupling dominated values as low as 5 fW/K at 50 mK. This value implies a fundamental thermal-energy-fluctuation limited noise level that is low enough for applications of great practical interest, in particular on-chip bolometric measurements in circuit quantum electrodynamics. Furthermore, we introduced a precise definition of differential thermal conductance in the presence of a parasitic heating term, which is non-negligible in many experiments at millikelvin temperatures. In future work, we will probe the thermal time constant and other non-steady-state properties of our nanobolometer.

We thank Tero Heikkilä for helpful discussions and Leif Grönberg for depositing Nb thin films on some samples. We also gratefully acknowledge the provision of facilities and technical support by Aalto University at Micronova Nanofabrication Centre and the financial support from Emil Aal-

tonen Foundation, the European Research Council under Grant 278117 ("SINGLEOUT"), Academy of Finland under Grants 141015, 272806, 135794, 260880, 138903, and 251748 ("COMP"), and the Finnish Cultural Foundation. We also thank all developers of the open-source lab environment QTLAB.

* joonas.govenius@aalto.fi

[1] B. Karasik, A. Sergeev, and D. Prober, IEEE Trans. Terahertz Sci. **1**, 97 (2011).
[2] D. J. Benford and Moseley, Nucl. Instrum. Methods Phys. Res., Sect. A **520**, 379 (2004).
[3] A. Blais, R. S. Huang, A. Wallraff, S. M. Girvin, and R. J. Schoelkopf, Phys. Rev. A **69**, 062320 (2004).
[4] A. Wallraff, D. I. Schuster, A. Blais, L. Frunzio, Huang, J. Majer, S. Kumar, S. M. Girvin, and R. J. Schoelkopf, Nature (London) **431**, 162 (2004).
[5] D. Riste, M. Dukalski, C. A. Watson, G. de Lange, M. J. Tiggelman, Y. Blanter, K. W. Lehnert, R. N. Schouten, and L. DiCarlo, Nature (London) **502**, 350 (2013).
[6] P. D. Nation, J. R. Johansson, M. P. Blencowe, and F. Nori, Rev. Mod. Phys. **84**, 1 (2012).
[7] J. Wei, D. Olaya, B. S. Karasik, S. V. Pereverzev, A. V. Sergeev, and M. E. Gershenson, Nature Nano. **3**, 496 (2008).
[8] B. S. Karasik and R. Cantor, Appl. Phys. Lett. **98**, 193503 (2011).
[9] M. Kenyon, P. K. Day, C. M. Bradford, J. J. Bock, and H. G. Leduc, Proc. SPIE **6275**, 627508 (2006).
[10] D. F. Santavicca, B. Reulet, B. S. Karasik, S. V. Pereverzev, D. Olaya, M. E. Gershenson, L. Frunzio, and D. E. Prober, Appl. Phys. Lett. **96**, 083505 (2010).
[11] B. S. Karasik, S. V. Pereverzev, A. Soibel, D. F. Santavicca, D. E. Prober, D. Olaya, and M. E. Gershenson, Appl. Phys. Lett. **101**, 052601 (2012).
[12] P. K. Day, H. G. LeDuc, B. A. Mazin, A. Vayonakis, and J. Zmuidzinas, Nature (London) **425**, 817 (2003).
[13] R. M. J. Janssen, J. J. A. Baselmans, A. Endo, L. Ferrari, S. J. C. Yates, A. M. Baryshev, and T. M. Klapwijk, Appl. Phys. Lett. **103**, 203503 (2013).
[14] M. Nahum and J. Martinis, Physica B **194**, 109 (1994).
[15] D. R. Schmidt, C. S. Yung, and A. N. Cleland, Appl. Phys. Lett. **83**, 1002 (2003).
[16] D. R. Schmidt, K. W. Lehnert, A. M. Clark, W. D. Duncan, K. D. Irwin, N. Miller, and J. N. Ullom, Appl. Phys. Lett. **86**, 053505 (2005).
[17] D. E. Prober, J. D. Teufel, C. M. Wilson, L. Frunzio, M. Shen, R. J. Schoelkopf, T. R. Stevenson, and E. J. Wollack, IEEE Trans. Appl. Supercond. **17**, 241 (2007).
[18] S. Komiyama, O. Astafiev, V. Antonov, T. Kutsuwa, and H. Hirai, Nature (London) **403**, 405 (2000).
[19] H. Hashiba, V. Antonov, L. Kulik, A. Tzalenchuk, and S. Komiyama, Nanotechnol. **21**, 165203 (2010).
[20] S. Komiyama, IEEE J. Sel. Top. Quant. Electr. **17**, 54 (2011).
[21] K. C. Fong and K. C. Schwab, Phys. Rev. X **2**, 031006 (2012).
[22] J. Yan, M.-H. Kim, J. A. Elle, A. B. Sushkov, G. S. Jenkins, H. M. Milchberg, M. S. Fuhrer, and H. D. Drew, Nature Nano. **7**, 472 (2012).
[23] M. Mittendorff, S. Winnerl, J. Kamann, J. Eroms, D. Weiss, H. Schneider, and M. Helm, Appl. Phys. Lett. **103**, 021113 (2013).
[24] C. B. McKitterick, D. E. Prober, and B. S. Karasik, J. Appl. Phys. **113**, 044512 (2013).
[25] Y. Kawano, T. Uchida, and K. Ishibashi, Appl. Phys. Lett. **95**, 083123 (2009).
[26] P. L. Richards, T. M. Shen, R. E. Harris, and F. L. Lloyd, Appl. Phys. Lett. **36**, 480 (1980).
[27] J. Bueno, M. D. Shaw, P. K. Day, and P. M. Echternach, Appl. Phys. Lett. **96**, 103503 (2010).
[28] K. J. Stone, K. G. Megerian, P. K. Day, P. M. Echternach, J. Bueno, and N. Llombart, Appl. Phys. Lett. **100**, 263509 (2012).
[29] J. E. Sadleir, S. J. Smith, S. R. Bandler, J. A. Chervenak, and J. R. Clem, Phys. Rev. Lett. **104**, 047003 (2010).
[30] F. C. Wellstood, C. Urbina, and J. Clarke, Phys. Rev. B **49**, 5942 (1994).
[31] J. B. Pendry, J. Phys. A **16**, 2161 (1983).
[32] K. Schwab, E. A. Henriksen, J. M. Worlock, and M. L. Roukes, Nature (London) **404**, 974 (2000).
[33] D. R. Schmidt, R. J. Schoelkopf, and A. N. Cleland, Phys. Rev. Lett. **93**, 045901 (2004).
[34] M. Meschke, W. Guichard, and J. P. Pekola, Nature (London) **444**, 187 (2006).
[35] S. Jezouin, F. D. Parmentier, A. Anthore, U. Gennser, A. Cavanna, Y. Jin, and F. Pierre, Science **342**, 601 (2013).
[36] L. M. A. Pascal, H. Courtois, and F. W. J. Hekking, Phys. Rev. B **83**, 125113 (2011).
[37] J. C. Mather, Appl. Opt. **21**, 1125 (1982).
[38] S. H. Moseley, J. C. Mather, and D. McCammon, J. Appl. Phys. **56**, 1257 (1984).
[39] N. E. Booth, B. Cabrera, and E. Fiorini, Annu. Rev. Nucl. Part. Sci. **46**, 471 (1996).
[40] F. Giazotto, T. T. Heikkilä, G. P. Pepe, P. Helistö, A. Luukanen, and J. P. Pekola, Appl. Phys. Lett. **92**, 162507 (2008).
[41] J. Voutilainen, M. A. Laakso, and T. T. Heikkilä, J. Appl. Phys. **107**, 064508 (2010).
[42] H. Okamoto and T. B. Massalski, Bull. All. Ph. Diagr. **6**, 229 (1985).
[43] J. T. Peltonen, P. Virtanen, M. Meschke, J. V. Koski, T. T. Heikkilä, and J. P. Pekola, Phys. Rev. Lett. **105**, 097004 (2010).
[44] E. V. Bezuglyi and V. Vinokur, Phys. Rev. Lett. **91**, 137002 (2003).
[45] P. Dubos, H. Courtois, B. Pannetier, F. K. Wilhelm, A. D. Zaikin, and G. Schön, Phys. Rev. B **63**, 064502 (2001).
[46] J. Voutilainen, P. Virtanen, and T. T. Heikkilä, Phys. Rev. Lett. **109**, 067002 (2012).
[47] M. Göppl, A. Fragner, M. Baur, R. Bianchetti, S. Filipp, J. M. Fink, P. J. Leek, G. Puebla, L. Steffen, and A. Wallraff, J. Appl. Phys. **104**, 113904 (2008).
[48] B. Dassonneville, M. Ferrier, S. Guéron, and H. Bouchiat, Phys. Rev. Lett. **110**, 217001 (2013).
[49] P. Virtanen, F. S. Bergeret, J. C. Cuevas, and T. T. Heikkilä, Phys. Rev. B **83**, 144514 (2011).
[50] P. L. Richards, J. Appl. Phys. **76**, 1 (1994).
[51] E. M. Gershenzon, G. N. Goltsman, A. I. Elantev, B. S. Karasik, and S. E. Potoskuev, Sov. J. Low Temp. Phys. **14**, 753 (1988).
[52] A. I. Elantev and B. S. Karasik, Sov. J. Low Temp. Phys. **15**, 379 (1989).
[53] B. S. Karasik, S. V. Pereverzev, D. Olaya, J. Wei, M. E. Gershenson, and A. V. Sergeev, IEEE Trans. Appl. Supercond. **19**, 532 (2009).
[54] J. T. Muhonen, M. Meschke, and J. P. Pekola, Rep. Prog. Phys. **75**, 046501 (2012).
[55] V. Chandrasekhar, Supercond. Sci. Technol. **22**, 083001 (2009).
[56] K. Y. Arutyunov, D. S. Golubev, and A. D. Zaikin, Phys. Rep.

**464**, 1 (2008).
[57] A. V. Timofeev, M. Helle, M. Meschke, M. Möttönen, and J. P. Pekola, Phys. Rev. Lett. **102**, 200801 (2009).
[58] J. T. Muhonen, A. O. Niskanen, M. Meschke, Yu, J. S. Tsai, L. Sainiemi, S. Franssila, and J. P. Pekola, Appl. Phys. Lett. **94**, 073101 (2009).
[59] H. Courtois, M. Meschke, J. T. Peltonen, and J. P. Pekola, Phys. Rev. Lett. **101**, 067002 (2008).
[60] J. Bardeen, G. Rickayzen, and L. Tewordt, Phys. Rev. **113**, 982 (1959).
[61] J. Aumentado, M. W. Keller, J. M. Martinis, and M. H. Devoret, Phys. Rev. Lett. **92**, 066802 (2004).
[62] P. J. de Visser, J. J. A. Baselmans, P. Diener, S. J. C. Yates, A. Endo, and T. M. Klapwijk, Phys. Rev. Lett. **106**, 167004 (2011).
[63] E. V. Bezuglyi, E. N. Bratus', V. S. Shumeiko, and G. Wendin, Physical Review B **63**, 100501 (2001).